RSC Advances

PAPER

View Article Online
View Journal | View Issue

Cite this: *RSC Adv.*, 2021, **11**, 39985

Proton-coupled electron transfer of catechin in tea wine: the enhanced mechanism of anti-oxidative capacity†

Yirong Xia,[a] Xintong Wang,[a] Hechen Sun[b] and Ximing Huang *[a]

Tea wine is a Chinese traditional alcoholic drink made by cereal and tea leaves. It is rich in tea polyphenols, caffeine, amino acids, and protons and possesses various healthcare functions. In this work, electrochemical methods, as well as density functional theory (DFT) calculations, were adopted to reveal the proton-coupled electron-transfer process of catechin in tea wine. The electrochemical results showed that the catechin preferred hydrogen-bonding with ethanol and formed molecular clusters. Thus, the direct electron-transfer process of catechin changed to proton-coupled electron transfer. This procedure reduced the energy barrier of the redox reaction and enhanced the anti-oxidative capacity. Subsequently, DFT calculations were employed to explore the bond length, bond energy, and HOMO–LUMO energy gap of catechin, which confirmed the above-mentioned mechanism. Our work offers some positive value for the scientific promotion of traditional food and a greater understanding of the health mechanisms in terms of chemistry.

Received 21st October 2021
Accepted 30th November 2021

DOI: 10.1039/d1ra07769d

rsc.li/rsc-advances

1. Introduction

China has a long history of wine-drinking to dispel wind and cold, as well as to prevent aspects of diseases effectively.[1] Simultaneously, tea-drinking is also a Chinese traditional custom due to its various healthcare functions promoted by polyphenol, caffeine and the like in tea.[2–5] On the basis of tradition, Chinese people creatively began to make wine with tea leaves and invented a new alcoholic drink: Chinese tea wine. During the process of making tea wine, most of the nutritional and functional components of the tea are dissolved in the wine, such that the drink integrates the advantages of both tea and wine, and has extremely high pharmacological and healthcare functions.[6–9]

Since tea wine is made from tea, it is unquestionable that tea polyphenol is one of the most important physiologically active substances in this alcoholic drink,[10,11] while catechin is one of the most abundant compounds in tea polyphenols. Because of the high anti-oxidative activity of catechin, it not only plays a very positive role in eliminating free radicals, but also plays a beneficial health role in preventing some diseases, which has aroused the great interest of researchers.[12,13] For instance, scientists have found that the administration of catechin would reduce the lactate levels during exercise and bring a performance-enhancing effect.[14] In addition, catechin has also been found to reduce the capacity of bacterial pathogens and forms the basis of a new approach for treating staphylococcal infections.[15] Furthermore, catechin has been proved to offer some of neuroprotective effects against neural injuries and neurodegenerative diseases and consequently, the molecular mechanisms responsible for the neuroprotection in various models have been well described.[16] The above functions of catechin can be attributed to its anti-oxidative capacity. It is worth noting that these investigations about catechin are usually conducted in the water phase. However, as to tea wine, the solvent is not only water, but also part ethanol. Whether the anti-oxidative capacity of catechin can be affected by the solvent effect of ethanol is still unclear. Thus, this work focused on the changes in the anti-oxidative capacity of catechin in a mixed solvent of water and ethanol.

The solvent effect is a common physical phenomenon, which has a huge impact on chemical properties, such as surface structure and chiroptical properties.[17–20] The weak interactions between the solvent and solute molecules, such as hydrogen bonds, will promote the formation of large molecular clusters and change the chemical properties. Moreover, direct electron transfer from the solute would often be induced by a solvent effect to change to proton-coupled electron transfer.[21–24] As to the tea wine, the catechin molecules are weakly polar, which mean they would dissolve better in ethanol than water,[25] according to the principle of like dissolves like. Structurally, the catechin molecules possess five hydroxyl groups, which offer protons to form hydrogen bonds.[26] Considering the molecular polarity and structure of catechin, molecular clusters may be

[a]School of Food and Chemical Engineering, Shaoyang University, Shaoyang, 422000, China. E-mail: Ximinghuang_SYU@163.com

[b]Shanxian Central Hospital, Heze, 274300, China

† Electronic supplementary information (ESI) available. See DOI: 10.1039/d1ra07769d

formed between catechin and ethanol by hydrogen bonds in tea wine. In theory, the solvent effect between catechin and ethanol would occur. However, how this affects the anti-oxidative activity of catechin needs to be further explored by experiments.

Therefore, in this work, electrochemical methods, as well as density functional theory (DFT) calculations, were adopted to reveal the enhance mechanism of the anti-oxidative capacity in tea wine. The use of DFT calculations could offer some information about the optimized geometries, charge, electron energy, and HOMO–LUMO energy gap, which can help to understand the reaction mechanism and hence these have been widely employed in lots of research.[27–29] The cyclic voltammetry (CV) and scanning electrochemical microscopy (SECM) results showed that the catechin preferred hydrogen-bonding with ethanol to form molecular clusters. Thus, the direct electron-transfer process of catechin would change to proton-coupled electron transfer. This procedure reduces the energy barrier of the redox reaction and enhances the anti-oxidative capacity. Subsequently, DFT calculations were employed to interpret the HOMO–LUMO energy gap of catechin and confirmed the above-mentioned mechanism. This research would offer a positive value for the scientific promotion of traditional food and a greater understanding of its health mechanism in terms of the chemistry.

2. Experimental section

2.1 Chemicals

(+)-Catechin hydrate (95%) and hydroxymethyl ferrocene (95%) were purchased from Aladdin (Shanghai, China). 2-Mercaptoethanol (99%) was purchased from Energy Chemical. Potassium phosphate monobasic (99.5%) and sodium phosphate dibasic dodecahydrate (99%) were purchased from Pageant. Sodium hydroxide (99%), hydrochloric acid (37%), ethanol (99.7%), and hydrogen peroxide (30%) were purchased from Chuandong chemical plant (Chongqing, China). Ultrapure water was prepared by water purifiers and used in all the experiments. All the chemicals were used without further purification.

2.2 Electrochemical experiments

Platinum ultra-micro working electrodes (radius 5 μm), Ag/AgCl (3 M KCl) reference electrodes, gold working electrodes, and platinum wire counter electrodes were purchased from CH Instruments, Inc. Scanning electrochemical microscopy (CHI 900D) was employed for all the electrochemical experiments. The potentials in all the experiments referred to the Ag/AgCl (3 M KCl) reference electrode.

The cyclic voltammograms of 10 mM catechin were conducted in a water solution of 0.2 M KCl on a gold electrode at pH 1.37, 2.02, 3.12, 4.43, 5.43, 6.42, 7.64, respectively, scanning from 0 to 0.8 V with a scan rate of 0.1 V s^{-1}. The cyclic voltammograms of 10 mM catechin were conducted on a gold electrode in the absence of ethanol and in the presence of 10% ethanol, respectively, with a scan rate of 0.1 V s^{-1}. The differential pulse voltammograms of 10 mM catechin were conducted on a gold electrode in the presence of 10%, 20%, 30%, 40%, 50%, 60%, 70%, 80%, 90% ethanol, respectively.

The approach curves of 1.0 mM ferrocenylmethanol towards the mercaptoethanol self-assembled monolayers were obtained in the absence of catechin and in the presence of 0.1 mM catechin, respectively. The tip electrode was biased with 0.4 V and the approach rate was set at 1 μm s^{-1}. The SECM images of the mercaptoethanol self-assembled monolayers in the absence and presence of catechin were obtained in a solution of 1.0 mM ferrocenylmethanol. The tip electrode was biased with 0.4 V, the tip to substrate distance was set $0.5d/a$, the scan rate was set 1 μm s^{-1} in the range of 10 μm × 10 μm.

Electrochemical impedance spectroscopy (EIS) was performed at an open circuit potential in the frequency range from 1000 to 106 Hz.

2.3 Scavenge hydroxyl radicals experiments

Here, 1 mL solution of ferrous sulfate (9 mmol L^{-1}) and salicylic acid (9 mmol L^{-1}) were added in to a water–ethanol solution of hydrogen peroxide (8.8 mmol L^{-1}) and catechin.[30,31] The mixture was placed in a 37 °C water bath for a specific time. The absorbance was measured at the light wavelength of 510 nm in parallel three times. The real samples of tea wine were prepared by adding catechin additionally in real commercial tea wine.

2.4 Self-assembled monolayers fabrication

First, a gold working electrode was polished by alumina powder to achieve a mirror surface. Later, the polished electrode was treated by ultrasound. Then, the clean electrode was immersed in 0.2 M H_2SO_4 and reactivated by an electrochemical method by cyclic voltammetry, where the potential was set from −0.2 to 1.6 V with a scan rate of 0.1 V s^{-1} to obtain the active gold surface. Lastly, the spotless gold working electrode was immersed in 0.05 M 2-mercaptoethanol for 24 h to obtain the self-assembled monolayers.

2.5 Density functional theory calculations

All the DFT calculations were performed with the Gaussian 16, Revision A.03 program package with the supercomputer in Liaoning Shihua University. DFT calculations were performed with the B3LYP method, and 6-311+g(d,p) basis sets for the C, H, and O atoms. The ground states of catechin, catechin–ethanol, and catechin–water clusters were optimized in the absence of solvent, while catechin–ethanol–water cluster calculations were performed in the water environment. Frequency calculations were also performed to make sure that the geometries of the ground-state reached the minimum point on the potential energy surfaces. All the computations were performed without symmetry constraints.

3. Results and discussion

3.1 Electrochemical behaviours of catechin

In the alcoholic drink tea wine, tea polyphenols are dissolved in water–ethanol solution and exhibit different properties by a solvent effect, where catechin is a major kind of phenolic active substance extracted from tea wine. It works in the body as an anti-oxidant and effectively scours free radicals.[32,33] In this

work, the first step was to elucidate the electrochemical behaviours of catechin. As to the polyphenols, the oxidation selectively occurred at the ring with low potential. The theoretical calculations to assess the stability of hydroxide radicals showed that 4′-OH and 3′-OH could be easily oxidized, whereas 7-OH and 5-OH were stable.[34,35] Thus, it was expected that we could verify the oxidation behaviour using an electrochemical method. Fig. 1(a) shows the cyclic voltammograms of 10 mM catechin in a water solution of 0.2 M KCl on a gold electrode at pH 1.37, 2.02, 3.12, 4.43, 5.43, 6.42, 7.64, respectively. It could be seen that the oxidative peak potential, as well as the reductive peak potential, decreased gradually as the pH increased. In addition, the oxidative current was still high at a potential of 0.5–0.7 V at pH 7.64, which could be attributed to the oxidation of the –OH group on the C ring at a low proton concentration.[35,36] Fig. 1(b) and (c) show plots of the oxidative and reductive peak potential *versus* pH, respectively. The electron and proton transfer dynamics can be analysed by the two figures. The slopes of the linear fitting curves were about −0.066 and −0.051, respectively, which were both close to −0.059. According to the Nernst equation, the relation between the peak potential and pH is as shown below:

$$\begin{aligned} E &= E^{\Theta} + \frac{0.059}{n}\log\frac{[\mathrm{Ox}]}{[\mathrm{Red}]} \\ &= E^{\Theta} + \frac{0.059}{n}\log\frac{[\mathrm{Oxcatechine}]\times[\mathrm{H}^+]^m}{[\mathrm{Redcatechine}]} \\ &= E^{\Theta} - 0.059\frac{m}{n}\mathrm{pH} \end{aligned} \quad (1)$$

where E^{Θ} is the formal potential, n is the number of electrons transferred in the reaction, m is the number of protons that participate in the reaction, [Oxcatechin] is the concentration of oxidative catechin, and [Redcatechin] is the concentration of reductive catechin. Our experiments showed that the slope was close to −0.059, indicating the value of m/n was 1. In other words, the same number of electrons and protons were released in the oxidation process and the same number of electrons and protons were acquired in the reduction process. The Nernst slope of 0.059 V showed the same number of electrons and protons transferred. Therefore, the redox reaction of catechin was as shown:

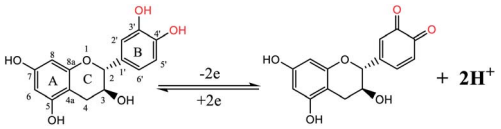

(2)

In addition, the electrochemical reversibility of catechin was also evaluated. Fig. 1(d) shows the plot of the ratio of the oxidative peak current to the reductive peak current *versus* pH. It was obvious that the ratio of the oxidative to reductive peak currents was approximately 1. Also, it could be seen from Fig. 1(a) that the peak separation varied between 100 and 200 mV at different pH, indicating the quasi-reversible electrochemical behaviour of catechin.

3.2 Enhancement of the anti-oxidative capacity of catechin in tea wine

After discussing the electrochemical property of catechin, we made an effort to reveal the anti-oxidation behaviour of catechin in tea wine. In comparison to tea water drink, tea wine is

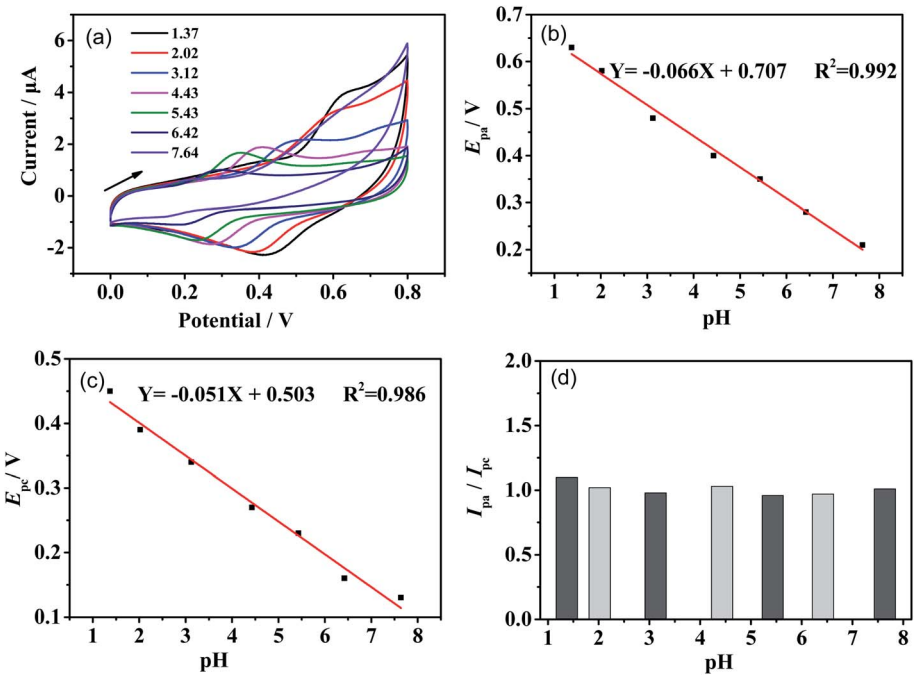

Fig. 1 (a) Cyclic voltammograms of 10 mM catechin in a water solution of 0.2 M KCl on a gold electrode at pH 1.37, 2.02, 3.12, 4.43, 5.43, 6.42, 7.64, respectively. Scan rate: 0.1 V s^{-1}. (b) Plot of the oxidative peak potential *versus* pH. (c) Plot of the reductive peak potential *versus* pH. (d) Plot of the ratio of the oxidative peak current to reductive peak current *versus* pH.

characterized by its mixed solvent of ethanol and water. It has been reported that the solvent effect has a great influence on the chemical properties of chemicals.[37,38] While in a mixed solution, the chemicals are often subject to a preferential solvent effect with one component, resulting in a specific electrochemical behaviour.[39] Therefore, we made a preliminary inference that the anti-oxidative capacity of catechin in tea wine would be different to that of tea water drink.

Electrochemical methods were adopted to exhibit the redox properties of tea wine. Fig. 2(a) shows the cyclic voltammograms of 10 mM catechin in the absence of ethanol (black line) and in the presence of 10% ethanol (red line), respectively. The relevant oxidative peak potential, reductive peak potential, and formal potential of the cyclic voltammograms are exhibited in Fig. 2(b). It could be seen that the cyclic voltammogram curves both expressed well reversible redox peaks of catechin in the presence and absence of ethanol. It is worth noting that the oxidative peak potential, reductive peak potential, and formal potential were all lower in the presence of 10% ethanol, compared to the case in the absence of ethanol. The shift in the oxidative peak to the left indicated that the oxidation process became easier, while the shift of the reductive peak to the left indicated that the reduction process became more difficult. Also, the lower formal potential indicated the lower energy barrier for redox reaction. So, it could be concluded that the catechin molecules exhibited greater anti-oxidative capacity in the presence of ethanol. Later, differential pulse voltammetry was adopted the reveal the role of the ethanol concentration on the redox behaviour of catechin. Fig. 2(c) shows the differential pulse voltammograms of 10 mM catechin in the presence of different ethanol concentrations (10–90%), respectively. As the concentration of ethanol increased, the peaks shifted to the left and got smaller. The plot of the oxidative peak potentials and currents *versus* ethanol concentration is shown in Fig. 2(d). The shift of the oxidative peak to the left indicated that the oxidation process became easier. In other words, the more ethanol the solution contained, the greater the anti-oxidative capacity the catechin possessed.

While, the oxidation peak currents became smaller in differential pulse voltammograms. Further, cyclic voltammograms of 1 mM catechin in the presence of different concentration of ethanol were conducted and the results are shown in Fig. S1 in the ESI.† The oxidative peak currents could be calculated by the following formula:[40,41]

$$I_{pa} = (2.69 \times 10^5)n^{3/2}SD^{1/2}Cv^{1/2} \quad (3)$$

where I_{pa} is the oxidative peak current, n is the number of electrons transferred, S is the area of the electrode, D is the diffusion coefficient, C is the concentration of redox species, and v is the scan rate. Thus, the diffusion coefficient of catechin could be calculated, as shown in Table S1 in the ESI.† It could be seen that the diffusion coefficient of catechin decreased gradually with the ethanol concentration increasing, which might be attributed to the solvent effect between ethanol and catechin. Thus, the slow release of the anti-oxidative capacity of catechin could be reached. Finally, the effect of the catechin concentration on the anti-oxidative capacity was investigated. Fig. S2(a)† shows the differential pulse voltammograms of different concentrations of catechin in 10% ethanol, respectively. It could

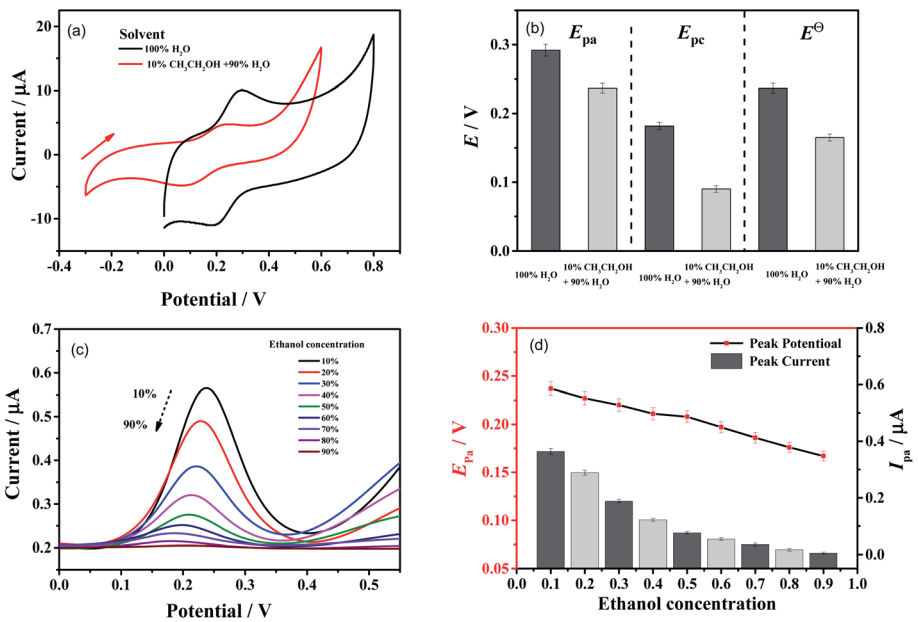

Fig. 2 (a) Cyclic voltammograms of 10 mM catechin in the absence of ethanol (black line) and in the presence of 10% ethanol (red line), respectively. Scan rate: 0.1 V s^{-1}. (b) Oxidative peak potential, reductive peak potential, and the formal potential of 10 mM catechin in the absence of ethanol (dark grey) and in the presence of 10% ethanol (light grey), respectively. (c) Differential pulse voltammograms of 10 mM catechin in the presence of different ethanol concentration, respectively. (d) Plot of the oxidative peak potential and current *versus* ethanol concentration, respectively.

be seen that the peak potentials did not exhibit an obvious shift, while the peak currents exhibited an obvious increase with the increasing concentration of catechin. The plot of the peak currents *versus* catechin concentration is shown in Fig. S2(b).† This result illustrated that the catechin concentration could change the amount of the oxidative reaction, instead of the degree of difficulty. To sum up, we employed cyclic voltammetry to reveal the anti-oxidation behaviour of catechin in the absence and presence of ethanol. The electrochemical results showed that catechin molecules exhibited greater anti-oxidative capacity and a slow-release ability in the presence of ethanol.

In order to inspect the real anti-oxidant and slow-release abilities of catechin, tea wine was prepared for scavenging free hydroxyl radicals in hydrogen peroxide solution. In this experiment, a 1 mL solution of ferrous sulfate (9 mmol L^{-1}) and salicylic acid (9 mmol L^{-1}) was added in to a water–ethanol solution of hydrogen peroxide (8.8 mmol L^{-1}) and catechin. The mixture was placed in a 37 °C water bath for a specific time. The absorbance was measured at the light wavelength of 510 nm in parallel three times. Thus, the clearance rate of hydroxyl radical could be calculated as below:

$$(^{\bullet}OH)\% = (A_0 - A_2 + A_1)/A_0 \times 100\% \quad (4)$$

where A_0 is the absorbance value of the blank solution, A_1 is the absorbance value of the hydrogen peroxide solution replaced by distilled water, and A_2 is the absorbance value of the solution after adding catechin. Fig. 3(a) shows the clearance rate of hydroxyl radicals by different concentrations of catechin in 10% and 50% ethanol, respectively. As shown in the graph, the clearance rate of hydroxyl radicals by catechin in 50% ethanol was obviously higher than that in 10% ethanol. This result was consistent with the electrochemical experiments showing that catechin molecules exhibited a greater anti-oxidant ability in the presence of more ethanol. Then, the slow-release ability of catechin in tea wine was inspected by the method of scavenging hydroxyl radicals. Fig. 3(b) shows the plots of the hydroxyl radical clearance rate (catechin concentration: 2mg mL^{-1}) *versus* time in 10% and 50% ethanol, respectively. It could be seen that the hydroxyl radical clearance rate gradually increased with time. The clearance rate was maximized at 240 min in 10% ethanol. However, it was maximized at 340 min in 50% ethanol. This result illustrated that the anti-oxidative capacity of catechin was released slowly in 50% ethanol, which was also consistent with the electrochemical experiments. Finally, the anti-oxidative capacity of catechin in real samples of tea wine was also investigated. Four real samples were prepared, and the clearance rates of hydroxyl radicals are shown in Fig. 3(c). Comparing the 1# and 2# samples, it could be seen that the increased ethanol led to an enhancement of the anti-oxidative capacity. Comparing the 1# and 3# samples, it could be seen that the additional added catechin could also enhance the anti-oxidative capacity. The 4# sample exhibited the highest anti-oxidative capacity due to the highest concentration of catechin and ethanol. The results for the real samples were consistent with the previous conclusion.

3.3 Proton-coupled electron transfer of catechin in tea wine

Through the above experiments, it was revealed that the anti-oxidative capacity of catechin could be enhanced in tea wine by the solvent effect of ethanol. Subsequently, the mechanism of the solvent effect should be well discussed. In theory, the catechin molecules were less polar, which meant they dissolved better in ethanol than water, according to the principle of like dissolves like. Structurally, the catechin molecules possessed five hydroxyl groups, which offered protons to form hydrogen bonds. Considering the molecular polarity and structure of catechin, it was speculated that molecular clusters might be formed between catechin and ethanol by hydrogen-bonding in tea wine. After the clusters were formed, the protons of the hydroxyl groups on catechin would be coupled with oxygen atoms on the ethanol molecules. This proton-coupled process could lead to the oxygen atoms of the hydroxyl groups on catechin becoming partially negative charged. Thus, during the catechin oxidation procedure, it was easier to lose protons and electrons. The catechin could be oxidized at a lower biased potential and showed a stronger anti-oxidative capacity. In addition, the formed molecular clusters would reduce the diffusion coefficient in solution, and as a result, a slower release

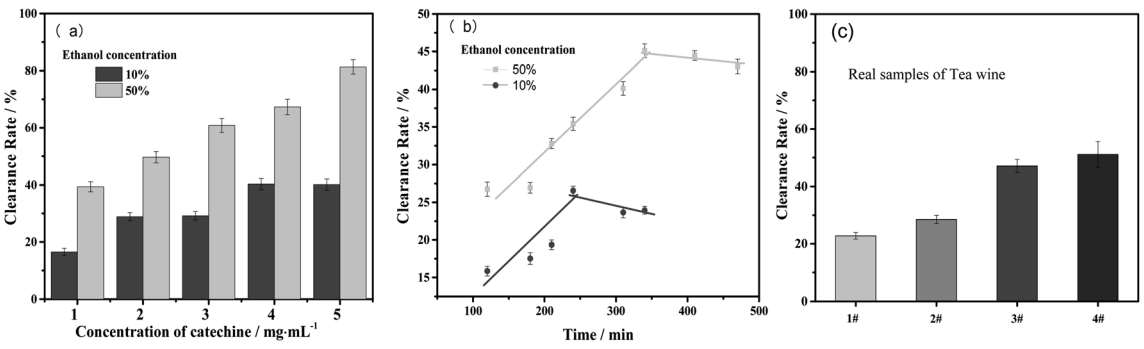

Fig. 3 (a) Clearance rate of hydroxyl radicals by different concentrations of catechin in 10% and 50% ethanol, respectively. (b) Plots of the hydroxyl radical clearance rate *versus* time in 10% and 50% ethanol, respectively. (catechin concentration: 2 mg mL^{-1}). (c) Clearance rate of hydroxyl radicals in real samples of tea wine. (1#, 43% ethanol, 1 mg mL^{-1} catechin; 2#, 50% ethanol, 1 mg mL^{-1} catechin; 3#, 43% ethanol, 3 mg mL^{-1} catechin; 4#, 50% ethanol, 3 mg mL^{-1} catechin).

ability could be reached. This hypothetical mechanism of proton-coupled electron transfer is summarized in Fig. 4.

Subsequently, SECM experiments were conducted to verify the hypothetical mechanism of catechin with ethanol in tea wine. In this part, ethanol with sulfhydryl groups, *i.e.* mercaptoethanol, was assembled on a gold electrode to build specific self-assembled monolayers by a spontaneous process. The use of self-assembled monolayers on gold is a popular in the field of constructing molecular scale membranes, because it can generate layers with well-defined packing and a density of specific molecules. It is often composed of a hydrophobic alkyl chain and a functional terminal group to achieve specific functions.[42–44] In this work, the mercaptoethanol self-assembled monolayers had lots of exposed hydroxyl groups. Subsequently, the electrochemical label, ferrocenylmethanol, was employed to probe the mercaptoethanol self-assembled monolayers in the absence and presence of catechin, respectively. The label molecules would oxidize on the tip of the electrode and diffuse to the gold substrate. When the gold substrate was assembled by mercaptoethanol, the reductive reaction of the oxidative label molecules would occur. The short chain length of mercaptoethanol allowed electrons to tunnel across the self-assembled monolayers. The reduced label molecules on the gold would increase the concentration around the tip, leading to the tip feedback current increasing significantly; whereas, if the solution contained catechin, the catechin would preferentially adsorb on the surface of mercaptoethanol self-assembled monolayers by hydrogen-bonding. Thus, the electron tunnelling would be weakened and the tip feedback current would not increase significantly. The scheme is summarized in Fig. 5(a).

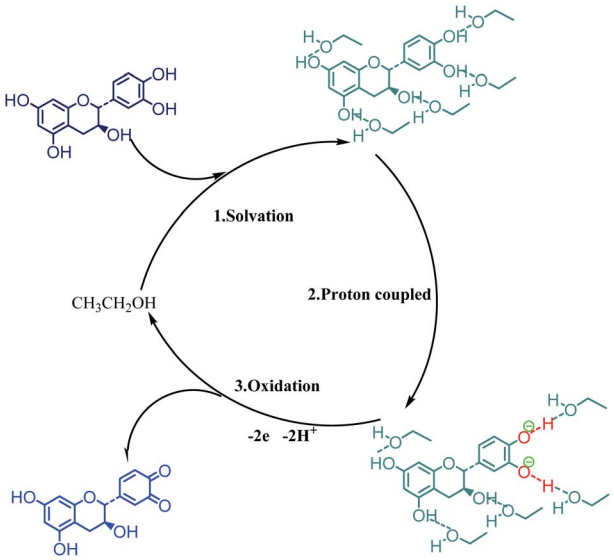

Fig. 4 Proton-coupled electron-transfer mechanism of catechin in tea wine.

The SECM curves for 1.0 mM ferrocenylmethanol towards the mercaptoethanol self-assembled monolayers in the absence

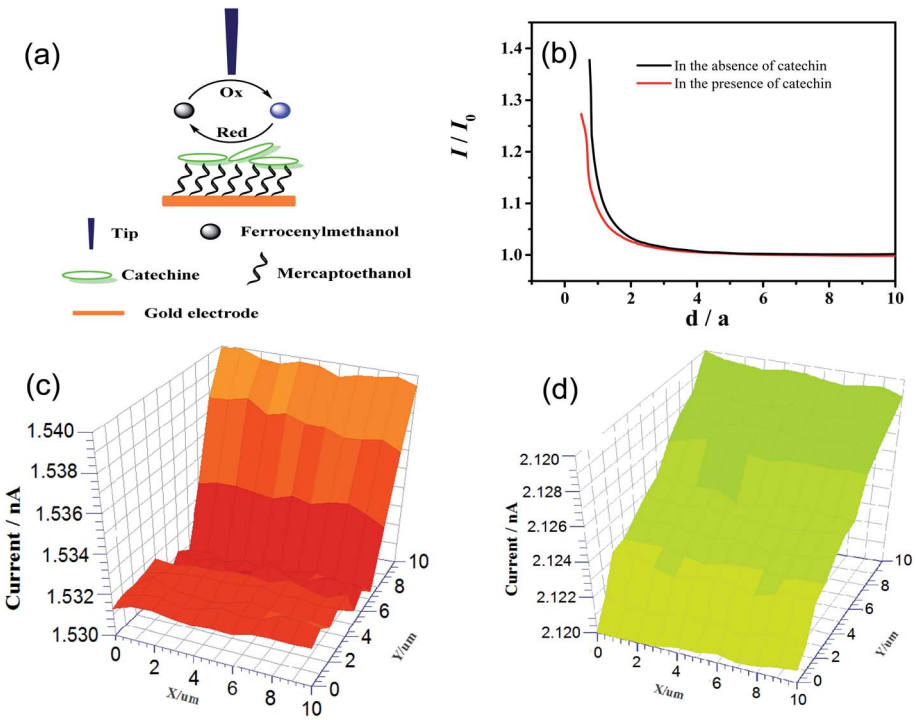

Fig. 5 (a) Scheme of scanning electrochemical microscopy for verifying the interaction between catechin and mercaptoethanol. (b) Approach curves of 1.0 mM ferrocenylmethanol towards the mercaptoethanol self-assembled monolayers in the absence of catechin and in the presence of 0.1 mM catechin, respectively. ($E_T = 0.4$ V, approach rate: 1 μm s^{-1}) (c) scanning electrochemical microscopy image of the mercaptoethanol self-assembled monolayers in the absence of catechin. (d) Scanning electrochemical microscopy image of the mercaptoethanol self-assembled monolayers in the presence of 0.1 mM catechin. (Tip to substrate distance, 0.5*d*/*a*; $E_T = 0.4$ V; scan rate, 1 μm s^{-1} in the range of 10 μm × 10 μm).

of catechin (black line) and in the presence of 0.1 mM catechin (red line) are shown in Fig. 5(b). It could be seen that the tip normalization current in the presence of catechin was lower than that in the absence of catechin at the same normalization distance. These results indicated that the electron tunnelling of label molecules was weakened once catechin was added in. This phenomenon conformed to the original design and verified that catechin would preferentially adsorb the molecules with hydroxyl groups. Fig. 5(c) and (d) show the SECM images of the mercaptoethanol self-assembled monolayers in the range of 10 μm × 10 μm, in the absence and presence of catechin, respectively. The tip currents were between 2.120 and 2.130 nA in the absence of catechin. However, the tip currents were between 1.530 and 1.540 nA in the presence of 0.1 mM catechin. These results illustrated that the catechin was adsorbed equally on the surface of the mercaptoethanol self-assembled monolayers. Subsequently, electrochemical impedance spectroscopy was adopted to confirm the interaction between catechin and ethanol. In this part, ethanol was also assembled on a gold electrode to build the mercaptoethanol self-assembled monolayers, and then electrochemical impedance spectroscopy was performed in the absence and presence of catechin, as shown in Fig. S3.† The curves showed that the charge-transfer impedance in the presence of catechin (223 ohm) was higher than that in the absence of catechin (198 ohm). This result indicated that catechin was adsorbed equally on the surface of the mercaptoethanol self-assembled monolayers, which was consistent with the SECM experiments.

The SECM experiments were able to verify the absorption between catechin and ethanol. Then DFT calculations were employed to further inspect the interactions between catechin and ethanol. In this section, the geometry optimization of catechin–ethanol cluster was conducted using the density functional theory at b3lyp/6-311+g(d, p),[45,46] with the help of Gaussian 16, Revision A.03. First, DFT calculations were conducted in a solvent-free environment. Also, the optimized geometries, charge, and electron energy of catechin (Structure A) and a catechin–ethanol cluster (Structure D) are shown in Fig. 6, respectively. It could be seen that the O–H bond length of 3′-OH and 4′-OH exhibited a slight increase after catechin was surrounded by ethanol, as shown in Table 1. Meanwhile, the catechin might also form hydrogen bonds with water molecules. The optimized geometry of a catechin–water cluster is shown in Fig. S4,† and the bond length of hydroxyl groups in catechin is also summarized in Table 1. It could be seen that the bond lengths of 3′-OH and 4′-OH in the catechin–water cluster were longer than that in catechin without forming a cluster, but shorter than that in the catechin–ethanol cluster. These results illustrated the solvation effect of ethanol on catechin was stronger than water.

The O–H bond energy of 3′-OH and 4′-OH could also be obtained. As to catechin, the O–H bond energy could be calculated as follows:

$$E = E_B + 2E_C - E_A \quad (5)$$

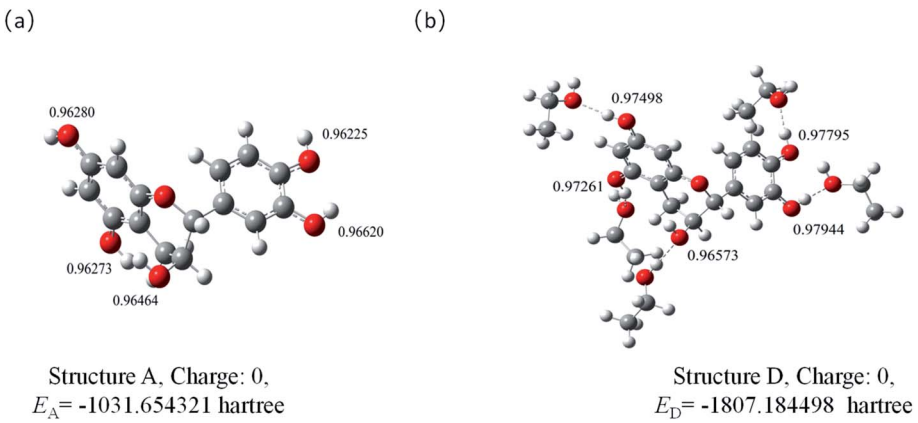

Fig. 6 Optimized geometries of catechin (a) and catechin–ethanol cluster (b).

Table 1 Bond length of hydroxyl groups in catechin before and after forming clusters

	3′-OH	4′-OH	3-OH	5-OH	7-OH
Bond length/Å, before cluster formation	0.96620	0.96225	0.96464	0.96273	0.96280
Bond length/Å, cluster formation with ethanol	0.97944	0.97795	0.96573	0.97261	0.97498
Bond length/Å, cluster formation with water	0.97631	0.97405	0.97416	0.97121	0.97233
Bond length/Å, cluster formation with ethanol in water environment	0.98350	0.98740	0.96605	0.97961	0.98296

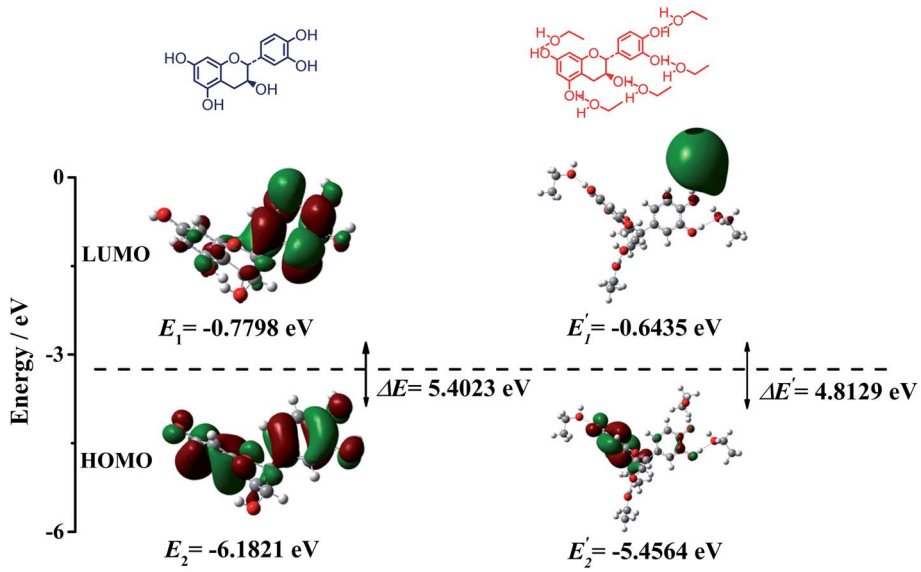

Fig. 7 HOMO–LUMO plots of catechin and the catechin–ethanol cluster, respectively.

where E_A, E_B, E_C are the electron energy of structures A, B, C, respectively. Also, the optimized geometries, charge, and electron energy of structures B and C are shown in Fig. S5.† The average O–H bond energy of 3′-OH and 4′-OH in catechin was obtained as 508.8860 kJ mol^{-1}.

As to the catechin–ethanol cluster, the O–H bond energy could be calculated as follows:

$$E = E_E + E_F - E_D \quad (6)$$

where E_D, E_E, E_F are the electron energy of structures D, E, F, respectively. Also, the optimized geometries, charge, and electron energy of structures E and F are shown in Fig. S5.† The average O–H bond energy of 3′-OH and 4′-OH in the catechin–ethanol cluster was obtained as 339.8475 kJ mol^{-1}. The increase in O–H bond length and decrease in O–H bond energy indicated the protons were easier to lose once the catechin was surrounded by ethanol. Fig. 7 shows the HOMO–LUMO plots of catechin and the catechin–ethanol cluster, respectively. The HOMO–LUMO energy gap of catechin was found to be 5.4023 eV, while the HOMO–LUMO energy gap of the catechin–ethanol cluster was found to be 4.8129 eV. The smaller energy gap indicated an easier electron transfer. Thus, it could be declared that the electron transfer of catechin had a lower energy barrier after the proton-coupled process. Finally, to make the model more realistic, the optimized geometry of a catechin–ethanol–water cluster in a water environment was assessed. The model is shown in Fig. S6† and the bond lengths of hydroxyl groups in catechin are also summarized in Table 1. It could be seen that the bond lengths of 3′-OH and 4′-OH were the longest compared to with other models. These results illustrated that the solvation effect of ethanol on catechin would be enhanced in a water environment. To sum up, DFT calculations were able to show that it was easier to lose protons and electrons and to exhibit stronger anti-oxidative capacity in the presence of ethanol during the catechin oxidation procedure.

4. Conclusion

In this work, the anti-oxidative capacity and the proton-coupled electron-transfer mechanism of catechin in tea wine was well inspected. Electrochemical experiments and scavenging hydroxyl radicals experiments were employed to explore the anti-oxidative capacity of catechin in tea wine. It was found that the anti-oxidative capacity was obviously enhanced, which was exhibited in two aspects: the greater anti-oxidative capacity and a slower release ability. The enhancements could be attributed to the proton-coupled electron-transfer mechanism of catechin in tea wine. The proton-coupled process induced the catechin molecule to more easily lose electrons and to exhibit a greater anti-oxidative capacity. Finally, DFT calculations were adopted and confirmed the above-mentioned proton-coupled electron-transfer mechanism.

Author contributions

Yirong Xia: Experiments, Data curation, Original draft preparation. Xintong Wang: Software. Hechen Sun: Reviewing and Editing. Ximing Huang: Conceptualization, Methodology, Validation.

Conflicts of interest

We declare that there is no conflict of interest including any financial, personal or other relationships with other people or organizations.

Acknowledgements

We gratefully acknowledge the financial support from National College Students' innovation and entrepreneurship training program (202110547021), Innovation Foundation for Postgraduate of Shaoyang University (CX2021SY070). We gratefully

acknowledge the Density Functional Theory calculation supported by Liaoning Shihua University.

References

1 W. Jia, Z. Fan, A. Du, Y. Li, R. Zhang, Q. Shi, L. Shi and X. Chu, *Food Chem.*, 2020, **324**, 126899.
2 M. E. Harbowy and D. A. Balentine, *Crit. Rev. Plant Sci.*, 1997, **16**, 415–480.
3 T. Karak and R. M. Bhagat, *Food Res. Int.*, 2010, **43**, 2234–2252.
4 S. M. Henning, P. Wang and D. Heber, *Mol. Nutr. Food Res.*, 2011, **55**, 905–920.
5 C. S. Yang, J. Ju, G. Lu, H. Xiao, X. Hao, S. Sang and J. D. Lambert, *Asia Pac. J. Clin. Nutr.*, 2008, **17**, 245–248.
6 Z. Shuai, *Sci. Tech. Food Ind.*, 2008, **29**, 162–164.
7 X. Qiu, L. Li, Q. Jiang, R. Xu, S. Xiao and X. Xiao, *Food Sci.*, 2010, **31**, 300–304.
8 X. Qiu, L. Li, Y. Ni, R. Xu and Q. Jiang, *J. Tea Sci.*, 2011, **31**, 537–545.
9 J. Wang, H. Yang, Y. Zhang, X. Wu, Z. Li and Z. Xu, *Food Ferm. Ind.*, 2018, **44**, 158–163.
10 Y. Li, S. Zhang and Y. Sun, *Saudi J. Biol. Sci.*, 2020, **27**, 214–221.
11 X. Zhao, H. Xu and R. Yang, *Food Sci.*, 2014, **35**, 169–175.
12 A. Ganeshpurkar and A. Saluja, *Indian J. Biochem. Biophys.*, 2020, **57**, 505–511.
13 M. Isemura, *Molecules*, 2019, **24**, 528.
14 M. M. Goktepe, M. Goktepe, E. Durukan, M. Gunay, F. Guder and M. Eraslan, *Prog. Nutr.*, 2020, **22**, e2020023.
15 P. W. Taylor, *Molecules*, 2020, **25**, 1986.
16 A. R. Khalatbary and E. Khademi, *Nutr. Neurosci.*, 2020, **23**, 281–294.
17 J. X. Chen, H. Z. Zhuang, J. Zhao and J. A. Gardella, *Surf. Interface Anal.*, 2001, **31**, 713–720.
18 C. W. Klampfl, *Electrophoresis*, 2003, **24**, 1537–1543.
19 B. Mennucci, C. Cappelli, R. Cammi and J. Tomasi, *Chirality*, 2011, **23**, 717–729.
20 B. L. Slakman and R. H. West, *J. Phys. Org. Chem.*, 2019, **32**, e3904.
21 S. C. Weatherly, I. V. Yang, P. A. Armistead and H. H. Thorp, *J. Phys. Chem. B*, 2003, **107**, 372–378.
22 A. Karkovic, C. J. Brala, V. Pilepic and S. Ursic, *Tetrahedron Lett.*, 2011, **52**, 1757–1761.
23 L. F. Cotter, B. P. Rimgard, G. A. Parada, J. M. Mayer and L. Hammarstrom, *J. Phys. Chem. A*, 2021, **125**, 7670–7684.
24 R. Tyburski, T. Liu, S. D. Glover and L. Hammarstrom, *J. Am. Chem. Soc.*, 2021, **143**, 560–576.
25 P.-T. Chuang, S.-C. Shen and J. S.-B. Wu, *J. Agric. Food Chem.*, 2011, **59**, 7818–7824.
26 W. Shim, C. E. Kim, M. Lee, S. H. Lee, J. Park, M. Do, J. Yang and H. Lee, *J. Controlled Release*, 2019, **307**, 413–422.
27 S. Wang, Z. Xu, Y. Wang and L. Tian, *Mol. Catal.*, 2021, 504.
28 J. Shen, M. J. Kolb, A. J. Gottle and M. T. M. Koper, *J. Phys. Chem. C*, 2016, **120**, 15714–15721.
29 J. Mao, P. Xu, Z. Zhou, Y. Zhou and Y. Tang, *J. Electrochem. Soc.*, 2021, 168.
30 J. T. K. Šmejkal, *Compr. Rev. Food Sci. F.*, 2016, **15**, 720–738.
31 J. Zhang, Q. Zhang, H. Li, X. Chen, W. Liu and X. Liu, *RSC Adv.*, 2021, **11**, 33872–33882.
32 I. E. Dreosti, *Nutrition*, 2000, **16**, 692–694.
33 T. Ohishi, R. Fukutomi, Y. Shoji, S. Goto and M. Isemura, *Molecules*, 2021, **26**, 453.
34 C. Cren-Olive, P. Hapiot, J. Pinson and C. Rolando, *J. Am. Chem. Soc.*, 2002, **124**, 14027–14038.
35 P. Janeiro and A. M. O. Brett, *Anal. Chim. Acta*, 2004, **518**, 109–115.
36 H. P. Hendrickson, A. D. Kaufman and C. E. Lunte, *J. Pharm. Biomed. Anal.*, 1994, **12**, 325–334.
37 X.-J. Wang, L. Wang, J.-J. Wang and T. Chen, *Electrochim. Acta*, 2007, **52**, 3941–3949.
38 M. Valter, B. Wickman and A. Hellman, *J. Phys. Chem. C*, 2021, **125**, 1355–1360.
39 C. Yan, X. Huang, J. Chen, H. Guo and H. Shao, *Electroanal*, 2019, **31**, 2339–2346.
40 T. Asakawa, H. Sunagawa and S. Miyagishi, *Langmuir*, 1998, **14**, 7091–7094.
41 X. X. Yuan and N. X. Xu, *J. Alloys Compd.*, 2001, **316**, 113–117.
42 S. Chattopadhyay, S. Bandyopadhyay and A. Dey, *Inorg. Chem.*, 2021, **60**, 598–606.
43 E. Hengge, M. Hirber, P. Brunner, E.-M. Steyskal, B. Nidetzky and R. Wuerschum, *Phys. Chem. Chem. Phys.*, 2021, **23**, 14457–14464.
44 S. Casalini, C. A. Bortolotti, F. Leonardi and F. Biscarini, *Chem. Soc. Rev.*, 2017, **46**, 40–71.
45 T. Beke, I. G. Csizmadia and A. Perczel, *J. Comput. Chem.*, 2004, **25**, 285–307.
46 A. R. Katritzky, N. G. Akhmedov, J. Doskocz, C. D. Hall, R. G. Akhmedova and S. Majumder, *Magn. Reson. Chem.*, 2007, **45**, 5–23.